AIAA 2003-1059

A New Method for Jet Noise Reduction in Turbofan Engines

D. Papamoschou
Dept. of Mechanical & Aerospace Engineering
University of California at Irvine
Irvine, CA

41st Aerospace Sciences Meeting & Exhibit
6-9 January 2003
Reno, Nevada

AIAA-2003-1059

A NEW METHOD FOR JET NOISE SUPPRESSION IN TURBOFAN ENGINES

Dimitri Papamoschou *
University of California, Irvine, Irvine, California 92697-3975

Jet noise suppression applicable to separate-flow turbofan engines is achieved by a slight downward tilt of the bypass plume relative to the core plume. The deflection results in a thick layer of secondary flow underneath the end of the potential core of the primary flow. It is believed that this layer reduces the convective Mach number of large eddies in the primary flow, thereby reducing their ability to generate sound that propagates to the downward acoustic far field. Noise reduction of around 5 dB in overall sound pressure level has been measured in a jet simulating the exhaust of a subsonic engine with bypass ratio 4.7. The present study investigates the mean velocity field of a coaxial jet with deflector vanes in the bypass stream and compares it to the velocity fields of other jets with axisymmetric and non-axisymmetric exit conditions. A comparison of special note is with the eccentric jet which has been investigated in the past. While the trends in both cases are similar, there are significant differences that may explain the acoustic superiority of the deflection approach. The paper also contains preliminary predictions of aerodynamic performance of the deflectors.

Nomenclature

a	=	speed of sound
A	=	cross sectional duct area
B	=	bypass ratio $= \dot{m}_s/\dot{m}_p$
D	=	diameter
F_x	=	axial force of vanes
F_y	=	transverse force of vanes
$\dot{m}$	=	mass flow rate
L	=	length of potential core
M	=	Mach number
M_c	=	convective Mach number
S	=	planform area of deflector vanes
$\mathcal{T}$	=	thrust
u	=	mean velocity in the plume or velocity inside duct
U	=	velocity at jet exit or in freestream
U_c	=	convective velocity
δ	=	deflection angle of bypass plume
θ	=	polar angle relative to jet axis
ρ	=	density

Subscripts

p	=	primary (core) exhaust
s	=	secondary (bypass) exhaust
v	=	vanes
∞	=	flight conditions

Introduction

Aircraft noise is an issue of enormous environmental, financial, and technological impact. There are two main sources of noise in today's commercial aircraft engines: fan/compressor noise and jet noise. Jet noise comprises turbulent mixing noise and, in the case of imperfectly expanded jets, shock noise [1]. Suppression of turbulent mixing noise remains a challenge as this type of noise is very difficult to control. It is widely agreed that turbulent shear-flow mixing causes two types of noise: sound produced by the convection of large-scale eddies and sound generated by fine-scale turbulence [2]. The former is very intense and propagates at an angle close to the jet axis. The latter is mostly uniform and affects mainly the lateral and upstream directions. Noise from fine-scale turbulence is typically 10 dB lower than noise from large-scale eddies. In large turbofan

*Professor, Associate Fellow AIAA

engines sound emitted by turbomachinery components may overshadow noise from fine-scale turbulence. Noise emitted in the aft quadrant, however, continues to be a strong contributor to overall aircraft noise.

Large-scale mixing noise has been successfully modeled by treating the large eddies as instability waves [1, 2, 3, 4]. A governing parameter is the convective Mach number M_c of the instability wave. When M_c is supersonic, strong Mach wave radiation is evident in instantaneous photographic realizations of jets. For subsonic M_c, the growth-decay nature of instability waves creates a spectrum of phase speeds, part of which is supersonic [2]. The resulting Mach wave emission is not as intense or nonlinear as its supersonic counterpart but still constitutes the strongest source of sound. As M_c becomes more subsonic, Mach wave emission (that is, the acoustic energy propagated to the far field by supersonic disturbances) weakens rapidly. This has spurred recent attempts to reduce M_c by strategic use of a secondary flow.

In a dual-stream jet, there are two convective Mach numbers that influence noise emission: one for the primary instability with respect to the secondary stream,

$$M_{c_p}(x) = \frac{U_{c_p}(x) - u_s(x)}{a_s(x)} \tag{1}$$

and the other for the secondary instability with respect to the ambient,

$$M_{c_s}(x) = \frac{U_{c_s}(x) - U_\infty}{a_\infty} \tag{2}$$

In coaxial jets the primary (core) jet is initially surrounded by the secondary (bypass) stream which acts as a moving medium. Given that the velocity ratio of these two flows is typically $U_s/U_p = 0.7$, one would expect dramatic reductions in the noise emitted by the core stream. This is not the case, however. In the coaxial exhaust of typical engines, the secondary stream becomes fully mixed well upstream of the end of the primary potential core. As a result, a substantial part of the core noise source region is not covered by the secondary flow. Figure 1 shows a prediction of potential core lengths for a turbofan engine with $B = 5$, based on the model of Murakami and Papamoschou [5]. The secondary potential core covers only 40% of the length of the primary potential core. The exposed region of the primary potential core thus contains strong sources of large-scale noise.

To counteract this undesirable feature of coaxial jets, experiments were conducted on offset nozzles with an eccentric exit geometry. The eccentric design improved the coverage of the primary noise source region by the secondary flow on the underside of the jet [5]. As a result, downward noise emission was reduced substantially. It became apparent, however, that offsetting the nozzles to an eccentric geometry did not offer an attractive engineering solution, particularly for high-bypass engines. Notwithstanding the possible losses caused by the new flow path, an eccentric arrangement would require an entirely new structure for the nacelle and would complicate installation of thrust reversers and other important systems.

An alternative was sought that would provide equal or greater acoustic benefit while minimizing modifications. A new configuration was thus developed that involved the placement of deflectors near the exit of the bypass stream of a coaxial exhaust [6]. The deflectors imparted a slight downward tilt to the bypass plume relative to the core plume, thus thickening the bypass stream near the end of the primary potential core. The rationale of this approach is summarized in Fig. 2. The acoustic benefit was superior to all the other non-axisymmetric arrangements tried.

The experiments of [6] thus introduced a new approach to reducing noise but also brought up some unresolved issues. Noise from an arcuate jet (Fig. 11(b)) - a geometry that seemed particularly promising – practically matched the noise from coaxial jet. The lack of noise reduction was puzzling. In addition, the coaxial configuration with vanes was consistently superior to the eccentric design. There were no obvious answer for this difference.

An important missing piece of the puzzle was the mean flow field. This report continues the work in [6] with emphasis on surveys of the mean velocity. In addition, it offers insights into the principle of the technique, discusses the impact on performance, and provides acoustic data with an alternative placement of the vanes.

Deflection of Bypass Stream

Working Principle

The rationale for tilting the bypass plume relative to the core plume is to thicken the bypass stream in the vicinity of the strongest sources of noise (largest eddies) of the core stream. The strongest sources of noise reside near the end of the primary potential core [10, 11]. Given that the length of the primary potential core is roughly 15 core exit diameters (Fig. 1), one can make an order-of-magnitude estimate that the desired tilt angle is a modest 1/15 or 4°. The tilt entails a transverse (lift) force F_y applied to the bypass stream near its exit. It can be created by vane-type deflectors or fluidic injection. Here we consider the former approach.

The vanes could be placed inside or outside the bypass duct. Placement inside the duct has the advantage of a subsonic environment and thus avoidance of any shock losses. There is a limit as to how deep inside the duct one should place the vanes. The key is that the aerodynamic force of the vanes should be transmitted to the momentum flux exiting the duct and not to the duct walls. Otherwise the effect of vane lift will be lessened or cancelled by transverse forces acting on the duct walls.

Aerodynamic Performance

The challenge of jet aeroacoustics is not noise reduction *per se* but noise reduction with acceptable performance penalty. For this reason, preliminary estimates are given for the aerodynamic performance of the deflectors. It is assumed that the deflectors are vanes (airfoils) rotated to a certain angle of attack when noise reduction is required and placed at zero angle of attack – or stowed – when noise reduction is not needed. The relations $\mathcal{T}_p = \dot{m}_p(U_p - U_\infty)$ and $\mathcal{T}_s = \dot{m}_s(U_s - U_\infty)$ are used in the analysis that follows.

Assuming that the lift of the vanes is transmitted entirely to the exhaust plume, Newton's second law (Fig. 3) gives that the tilt angle of the bypass stream is

$$\tan\delta \;=\; \frac{F_y}{\mathcal{T}_s}\left(1 - \frac{U_\infty}{U_s}\right)$$

The ideal thrust loss of the bypass stream is connected to the cosine of the tilt angle,

$$\frac{F_x}{\mathcal{T}_s} \;=\; \frac{1-\cos\delta}{1 - U_\infty/U_s}$$

For small tilt angle, $\tan\delta \approx \delta$ and $\cos\delta \approx 1 - \frac{1}{2}\delta^2$. It is easy to show that the ideal lift-to-drag ratio of deflectors is

$$\left(\frac{F_y}{F_x}\right)_{\text{ideal}} \;\approx\; \frac{2}{\delta} \qquad (\delta \text{ in radians})$$

The ideal thrust loss for the entire engine is

$$\left(\frac{F_x}{\mathcal{T}_{\text{total}}}\right)_{\text{ideal}} \;=\; \frac{BU_s(1-\cos\delta)}{U_p - U_\infty + B(U_s - U_\infty)} \qquad (3)$$

Treating the lift-to-drag ratio of the vanes, F_y/F_x, as an independent variable,

$$\frac{F_x}{\mathcal{T}_{\text{total}}} = \tan\delta\;\frac{F_x}{F_y}\;\frac{BU_s}{U_p - U_\infty + B(U_s - U_\infty)} \qquad (4)$$

This relation can be used to estimate the actual thrust loss given the tilt angle and the lift-to-drag ratio of the vanes.

To make some numerical estimates of performance with the vanes activated, we consider an engine similar to the General Electric CFM56 ($B = 5$) at take-off conditions. Flight velocity is $U_\infty = 100$ m/s and the exhaust speeds are $U_p = 480$ m/s and $U_s = 330$ m/s. Figure 4 plots the overall thrust loss for the ideal case and for vane lift-to-drag ratios of 5, 10, and 15. It is seen that, even for a poorly performing airfoil with $F_y/F_x = 5$, the overall thrust loss is around 1-2%. With the vanes placed inside the bypass duct, in a subsonic environment and accelerating flow, it should be possible to achieve lift-to-drag ratios exceeding ten and approaching the ideal case. In that case the thrust loss could become as low as 0.5%.

The above relations of course do not apply to the zero deflection case. When noise reduction is not required, the vanes could be either stowed flush with the nacelle or placed at zero angle of attack. The former method would produce zero thrust loss but probably entails more mechanical complexity than the latter one. Thrust loss at zero angle of attack stems from the parasite drag of the vanes. A microscopic treatment of vane drag gives

$$F_x \;=\; N_v C_D \frac{1}{2}(\rho u^2 S)_v$$

where N_v is the number of vanes, S_v is the planform area of each vane, and C_D is the vane drag

coefficient. As a fraction of the secondary thrust, the vane drag is

$$\frac{F_x}{\mathcal{T}_s} = \frac{N_v C_D}{2} \frac{u_v}{U_s - U_\infty} \frac{S_v}{A_v}$$

and the overall thrust loss is

$$\frac{F_x}{\mathcal{T}_{\text{total}}} = \frac{N_v C_D}{2} \frac{S_v}{A_v} \frac{B u_v}{U_p - U_\infty + B(U_s - U_\infty)} \quad (5)$$

An engine cycle analysis [7] was used to compute the exhaust conditions for an engine like the General Electric CFM56 at $M_\infty = 0.8$ ($U_\infty = 250$ m/s) cruise. The exit velocities are $U_p = 700$ m/s and $U_s = 400$ m/s. The vane configuration reflects the experimental arrangement of the next section: $N_v = 4$, $u_v = 180$ m/s, and $S_v/A_v = 0.07$. Substituting in Eq. 5,

$$\frac{F_x}{\mathcal{T}_{\text{total}}} = 0.1 C_D$$

A reasonable estimate for drag coefficient at zero lift is 0.01. Therefore the overall thrust loss in on the order of 0.1%. Figure 5 offers a more general result by plotting the thrust loss versus drag coefficient for various values of the total normalized vane area $N_v S_v / A_v$ and for the aforementioned exhaust conditions.

Sample Acoustic Data

Previous work on this noise suppression method [6] considered installation of vanes at the exit or past the exit of the bypass duct. Reductions in peak OASPL of 6 and 5 dB were measured for jets with bypass ratios 1.7 and 4.7, respectively. The current work examines placement of vanes inside the bypass duct and in the proximity of its exit. At that location, flow is high-subsonic and accelerating. The subsonic nature of the flow mitigates shock losses that increase the drag of the vanes. The favorable pressure gradient may allow use of thin airfoils at high angle of attack without the risk of flow separation.

Experiments were conducted at UCI's Jet Aeroacoustics Facility, described in earlier publications [8]. Mixtures of helium and air were used to simulate the exhaust conditions of a turbofan engine with bypass ratio 4.7. The nozzle design is shown in Fig. 6. At the nozzle exit, the plug diameter was 10 mm, the core diameter was 14 mm, and the bypass diameter was 23.4 mm. Exhaust conditions were $U_p = 480$ m/s, $M_p = 0.90$ for the core stream and $U_s = 330$ m/s, $M_s = 0.97$ for the bypass stream.

Four turning vanes were installed inside the bypass duct at a location where the Mach number was about 0.6. Figure 7 shows the coordinates of the bypass duct, the placement of vanes, and the axial Mach number distribution. The vane dimensions were 4.5×4.5 mm and their angle of attack was 20°. The vane width occupied practically the entire thickness of the annular duct. With $\phi = 0$ indicating the downward vertical direction, the vanes were placed at azimuth angles $\phi = \pm 75°$ and $\pm 105°$.

Comparisons were made between the acoustic far fields of the clean coaxial jet and of the coaxial jet with vanes. Figure 8 presents the noise spectra at polar emission angles of 25° and 40°. The frequency axis has been scaled to a full-size engine (scale factor of 50). At full-scale frequencies of around 500 Hz the deflection produces a benefit of 7 dB at θ=25° and 5 dB at θ=40°. A very important feature of this technique is that it reduces the spectrum across all frequencies. This is in contrast to vortex generators which reduce the low-frequency part of the spectrum but increase the high-frequency part of the spectrum [9].

The benefit of the deflection approach is also evident in the overall sound pressure level, plotted in Fig. 9, where a 5-dB drop in the peak OASPL is noted. This reduction is similar to that obtained with the vanes outside the bypass duct [6]. Figure 10 presents estimates of perceived noise level (PNL) versus time for a twin-engine aircraft climbing at an angle of 12°. The thrust of each engine is 90 kN. The effective perceived noise level (EPNL), a metric commonly used for aircraft noise, drops by 2.8 dB with deflection of the bypass stream. For further details on the PNL calculation the reader is referred to [12].

Mean Velocity Surveys

The purpose of these experiments was to study the mean flow fields of dual-stream jets consisting of a round primary flow surrounded by axisymmetric and non-axisymmetric secondary flows. It was desired to look not only at the case with vanes in the secondary stream but also to predecessor arrangements, namely nozzles with eccentric and arcuate exit configurations [6]. As mentioned in the introduction, the eccentric nozzle suppresses noise quite

effectively but the arcuate one does not.

Experimental Setup

Experiments were conducted in UCI's dual stream jet facility [8]. Mean flow surveys using Pitot probes require long run times which render the use of helium prohibitively expensive. For this reason, compressed air, supplied at room temperature, was used in both the core and bypass streams. The core stream exhausted at $M_p = 1.00$ ($U_p = 310$ m/s) and the bypass stream exhausted at $M_s = 0.66$ ($U_s = 220$ m/s). The resulting velocity ratio was U_s/U_p=0.7 which is representative of turbofan exit conditions at takeoff power. Thus the experiments matched the most important parameter that governs shear-layer mixing but did not capture the density ratio and convective Mach number of realistic exhausts.

Figure 11 shows perspective views of the dual-stream nozzles and the coordinate system used in the mean flow surveys. All the flows used the same core nozzle, which was convergent and terminated in a diameter of 14.8 mm and lip thickness of 0.7 mm. The coaxial and eccentric configurations used a round bypass nozzle with exit diameter 23.4 mm. The arcuate nozzle featured a smooth transition from a full annulus at the nozzle entrance to a 240° annulus at the nozzle exit. The outside diameter of the annulus was 26.3 mm. Two square vanes were mounted inside the bypass duct of the coaxial arrangement at azimuth angles $\phi = \pm 90°$, as shown in Fig. 11(d). Their width was equal to the thickness of the annular bypass duct and their trailing edges coincided with the duct exit. The vane angle of attack was 20°. All the nozzles shared the same secondary exit cross sectional area. The bypass ratio of all the dual stream jets was 1.0. The Reynolds number of the primary jet was 0.5×10^6.

A Pitot rake was used to survey the total pressure in the jet plume. The rake consisted of an aerodynamically shaped aluminum body encasing five stainless steel Pitot probes, each 75 mm long. The probes were mounted 10.2 mm apart allowing an overall sampling width of 51 mm. The inlet of each probe had a diameter of 1.0 mm. The rake was mounted on a carriage with motorized motion in the y direction and manual positioning in the x and z directions. For each axial (x) location the rake traversed the plume in the y direction a total of four times. Each time, the rake was moved by a $z-$increment of 2.54 mm, i.e., one fourth of the probe spacing. This resulted in 20 z locations being surveyed for each x. The survey resolution was 2.54 mm ($0.17D_p$) in z and 1.0 mm ($0.07D_p$) in y. A total of 18-23 $x-$locations were surveyed for each case, with x/D_p ranging from 0 to 18. Thus, each jet required a total of about 90 traverses of the Pitot rake.

The five probes of the rake were connected individually to five pressure transducers (Setra Model 207). The transducers were mounted on the traverse assembly in order to minimize the length of the tubing between each probe and transducer. This arrangement reduced the response time of the probe-transducer system to values low enough to resolve the sharp spatial in Pitot pressure near the nozzle exit. The carriage speed was 10 mm/s and the transducers were sampled each at 1000 samples per second by an analog-to-digital board. Each $y-$ traverse resulted in 8000 samples. Mach number and velocity were computed from the total pressure assuming constant total temperature (equal to room temperature) and uniform static pressure.

In addition to the Pitot pressures, the total pressures of the primary and secondary streams were measured by pressure transducers sampled at the same rate as the Pitot transducers. All seven transducers were calibrated before each experiment.

Axial Velocity Distribution

To get an overall picture of the flow development, Figure 12 plots the axial distributions of mean velocity at $y = 0$, $z = 0$. For each flow, the length of primary potential core, L_p, is defined from the relation $u(L_p, 0, 0) = 0.9U_p$. It takes the values $L_p = 8.1D_p$ for the single jet; $13.3D_p$ for the coaxial jet; $10.4D_p$ for the arcuate jet; $8.2D_p$ for the eccentric jet; and $11.6D_p$ for the coaxial jet with vanes in the bypass stream. The primary potential core of the coaxial jet is thus 1.6 times longer than that of the single jet. The eccentric jet mixes almost as fast as the single jet. The mixing rate of the arcuate jet is about halfway between that of the coaxial jet and the single jet. The potential core length of the coaxial jet with vanes is only 13% shorter than that of the clean coaxial jet. It was previously thought that the misalignment of the bypass and core flows would generate intense mixing rivaling that of the eccentric case [6]. Given the superior noise characteristics of the jet with vanes, the fact that the vanes did not produce substantial mixing enhancement was sur-

prising at first. Examination of the complete flow field in the next paragraphs will show that what really matters is the relative coverage of the primary flow by the secondary flow, not the absolute values of the potential core lengths.

$x-y$ Velocity Isocontours

Figure 13 presents iso-contour plots of $u(x,y,0)$ for all five cases covered in this experiment. Note again the dramatic elongation of the potential core with addition of the annular secondary flow. In the coaxial and arcuate cases, the secondary flow covers only the initial portion of primary potential core and does not cover the end of the potential core. This explains why noise emitted from the arcuate jet (in the direction $-y$) practically matched the noise emitted by the coaxial jet [6]. In the eccentric and vane cases, the secondary flow becomes very thick on the underside of the jet. The thick secondary layer covers all of the primary potential core. It is notable that, even though the coaxial jet with vanes mixes slower than the eccentric jet, the relative coverage of the primary flow by the secondary flow is roughly the same in both cases. This will become more evident in the plots that follow.

$y-z$ Velocity Isocontours

We now slice the velocity field along several $y-z$ planes. Figure 14 shows iso-contour plots of $u(x_0,y,z)$ for the four dual-stream jets, with x_0/D_p=8,12, and 16. The arcuate jet shows only minor asymmetry compared to the coaxial case and there is no discernible thick region of the secondary flow. Again, this explains why the arcuate jet was as noisy as the coaxial jet. The eccentric and vane arrangements show a substantial concentration of secondary flow on the underside of the jet. Given that most of the large-scale noise is generated near the end of the potential core [10, 11], we compare in Fig. 15 the $y-z$ isocontours of velocity of the eccentric and vane cases at the location where $u(x,0,0)=0.9U_p$. While the overall pattern is similar, there are important differences. The thick region on the underside of the eccentric jet is dominated by flow at $u/U_p \approx 0.7$ (close to the exit velocity of the bypass stream). The corresponding region of the coaxial jet with vanes is dominated by flow at $u/U_p \approx 0.5$. The contours in the eccentric case are pear-shaped while the contours in the coaxial jet with vanes have the shape of an upside-down tear drop. Even though this suggests that the eccentric case has better sideline acoustics, preliminary experiments show that the coaxial jet with vanes achieves about the same sideline (45-deg azimuth) noise reduction as the eccentric case. Nevertheless, the plots of Fig. 15 give strong hints as to how to improve sideline noise reduction. Options include changing the azimuthal location of the vanes, varying their "dihedral" angle, and even changing the nozzle shape.

Transverse Velocity Profiles

To gain further insight into the relative coverage of the primary flow by the secondary flow, we plot in Fig. 16 the transverse velocity profiles $u(L_p,y,0)$. The plot comprises the clean coaxial jet, the eccentric jet, and the coaxial jet with vanes. Recall that the primary potential core length, L_p, varies for the various jets. For the clean coaxial jet, there is no indication of a secondary layer; it has been fully mixed with the primary flow well upstream of the end of the potential core. In the eccentric and vane cases, there is a distinct layer on the underside of the jet. In both cases it is characterized by a flat, or nearly flat, portion followed by a slow decay along $-y$. The velocity of the "flat" portion is $u/U_p=0.7$ for the eccentric case and $u/U_p=0.5$ for the coaxial jet with vanes. This could turn out to be an important difference between the two cases. The layer on the underside of the eccentric jet contains a potential portion. The corresponding layer for the coaxial jet with vanes is not potential, since the velocity of its "flat" portion is less than the exit velocity of the secondary stream. It appears that the vanes create an induction of secondary flow from the top of the jet to the bottom of the jet. The process may not be isentropic, however this does not diminish the capacity of the resulting layer to suppress the large-scale sources of noise in the primary flow. The use of deflector vanes could in fact provide control over the extent of the secondary layer and its velocity distribution. This type of control is not possible by just offsetting the nozzles.

To explain the importance of controlling the velocity of the secondary layer, let us adopt for a moment the very simple view that the basic function of the secondary layer is to "break down" the velocity difference between the jet and the ambient into two steps: $\Delta U = r\Delta U + (1-r)\Delta U$. Assuming a power law dependence between noise intensity and veloc-

ity difference, and that noise from the two sources is uncorrelated, it is clear that $r = 0.5$ yields the least noise. For the eccentric case, $r = 0.8$ while in the case with the vanes $r = 0.6$. This could be one explanation for the quieter nature of the jet with vanes. Another way to look at it is that, in the eccentric case, the primary jet becomes very quiet but the secondary flow is noisy. In fact, past experiments have shown that, for frequencies relevant to annoyance, the acoustic field of the eccentric jet is dominated by noise produced by the secondary flow [12]. The coaxial jet with vanes seems to achieve a better balance between silencing the primary jet and maintaining a relatively quiet secondary flow. This argument would become more complete by considering the volume of noise sources in each flow. For an engine with large bypass ratio, the noise sources of the bypass stream would weigh more than those of the primary stream, yielding an optimal r of less than 0.5.

Concluding Remarks

This paper describes a noise reduction technique which is different in nature from methods employed today. Its basic principle is reduction of the convective Mach number near the end of the potential core of the jet. The most effective and practical way to achieve this reduction is via a modest downward deflection of the bypass stream relative to the core stream. As a result, a thick layer of secondary flow forms under the end of the primary potential core. The effect of the layer is to reduce the relative velocity of large eddies in that region and thus suppress noise.

The deflection is achievable with vanes installed inside or outside the bypass duct. The thrust loss caused by the vanes is estimated to be on the order of 1% with the vanes activated and 0.1% with the vanes at zero angle of attack. If the vanes could be folded into the nacelle, the cruise thrust loss would be zero. Aeroacoustic experiments simulating a subsonic engine with bypass ratio 4.7 show a substantial and across-the-board reduction of the spectra in the downward direction of peak sound emission.

Mean velocity surveys compare the flow field of the jet with vanes in the bypass stream to those of other axisymmetric and non-axisymmetric configurations. A comparison of special note is with the eccentric jet which has been investigated in the past. Even though the coaxial jet with vanes mixes slower than the eccentric jet, the relative coverage of the potential core by the secondary flow is roughly the same. Near the end of the potential core, the velocity ratio between the primary stream and the secondary layer is about 0.6 for the coaxial jet with vanes and 0.8 for the eccentric jet. It is argued that the eccentric jet has a noisy secondary flow, while the coaxial jet with vanes achieves a better balance between noise suppression for the primary flow and noise emission from the secondary layer.

The velocity surveys have shed light on the mechanism of noise suppression and explain why certain configurations of the past did not work. It is now evident that effective noise suppression entails a thick and slow secondary layer near the end of the primary potential core. The surveys also provide valuable guidance for improving this technique through parametric optimization. Parameters include the geometry of the vanes, their axial and azimuthal locations, and even the nozzle shape. Application of the vanes on elliptical bypass ducts and on partially-offset nozzles are possibilities.

Special Notice

The method and apparatus of noise suppression via deflection of the bypass and/or core streams is proprietary to the University of California. U.S. Patent Pending.

Acknowledgments

The support by NASA Glenn Research Center is gratefully acknowledged (Grant NAG-3-2345 monitored by Dr. Khairul B. Zaman). Mr. Thomas T. Dixon and Ms. Kimberley Nishi are thanked for their contributions to the experiments and data analysis.

References

[1] Tam, C.K.W., and Chen, P., "Turbulent Mixing Noise from Supersonic Jets," *AIAA Journal*, Vol. 32, No. 9, 1994, pp. 1774-1780.

[2] Tam, C.K.W., "Jet Noise: Since 1952," *Theoretical and Computational Fluid Dynamics,*" Vol. 10, 1998, pp. 393-405.

[3] Crighton, D.G. and Huerre, P., "Shear-Layer Pressure Fluctuations and Superdirective Acoustic Sources," *Journal of Fluid Mechanics*, Vol. 220, 1990, pp. 355-368.

[4] Avital, E.J., Sandham, N.D, and Luo, K.H., "Mach Wave Radiation in Mixing Layers. Part I: Analysis of the Sound Field," *Theoretical and Computational Fluid Dynamics*, Vol. 12, 1998, pp. 73-90.

[5] Murakami, E., and Papamoschou, D. "Mean Flow Development of Dual-Stream Compressible Jets," *AIAA Journal*, Vol. 40, No. 6, 2002, pp. 1131-1138.

[6] Papamoschou, D., "Noise Suppression in Moderate-Speed Dual-Stream Jets," AIAA-2002-2557.

[7] Papamoschou, D., "Engine Cycle and Exhaust Configurations for Quiet Supersonic Propulsion," AIAA-2002-3917.

[8] Papamoschou, D. and Debiasi, M., "Directional Suppression of Noise from a High-Speed Jet," *AIAA Journal*, Vol. 39, No. 3, 2001, pp. 380-387.

[9] Hileman, J., and Samimy, M. "Effects of Vortex Generating Tabs on Noise Sources in an Ideally Expanded Mach 1.3 Jet," AIAA-2002-2482.

[10] Hileman, J. and Samimy, M. "Turbulence Structures and the Acoustic Far Field of a Mach 1.3 Jet," *AIAA Journal*, Vol.39, No.9, 2001, pp.1716-27.

[11] Narayanan, S., Barber, T.J., and Polak, D.R., "High Subsonic Jet Experiments: Turbulence and Noise Generation Studies," *AIAA Journal*, Vol. 40, No. 3, 2002, pp. 430-437.

[12] Papamoschou, D. and Debiasi, M., "Mach Wave Elimination Applied to Turbofan Engines," AIAA-2002-0368; to appear in the *AIAA Journal of Propulsion and Power.*

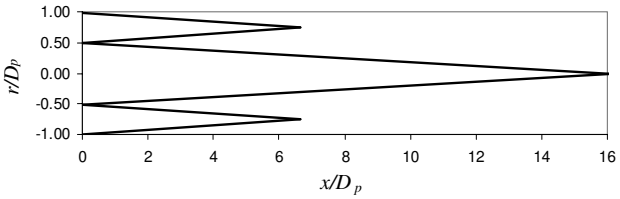

Fig.1 Potential core lengths of the exhaust of a subsonic engine with bypass ratio 5.

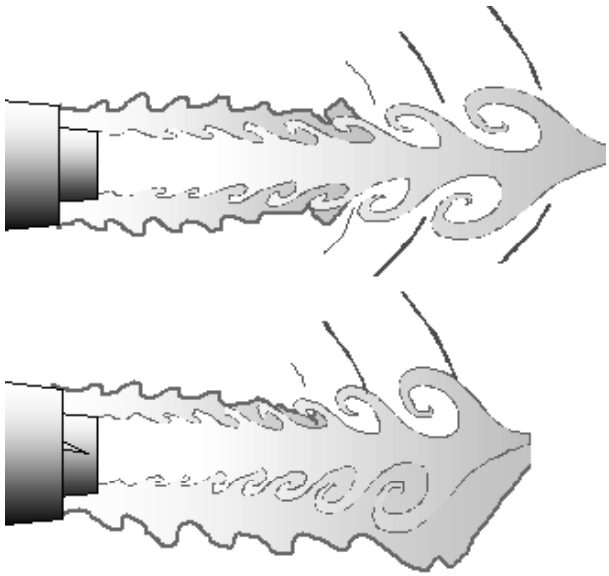

Fig.2 Illustration of the working principle of the noise suppression method. Top: no deflection; bottom: deflection of bypass stream.

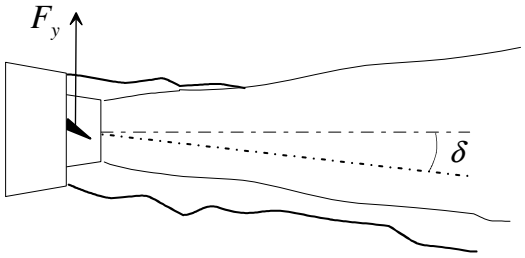

Fig.3 Basic physics of tilting of the bypass stream.

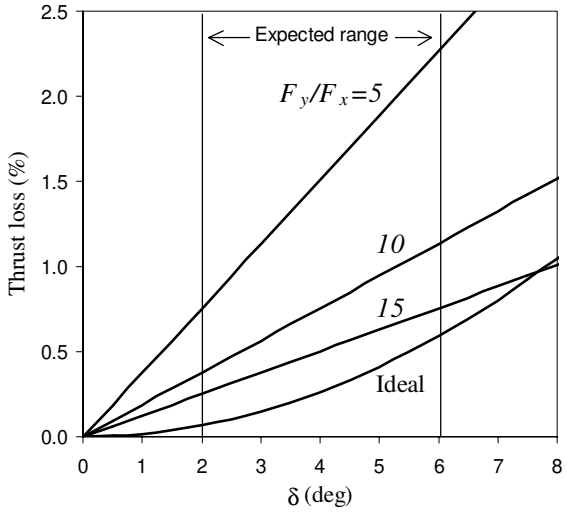

Fig.4 Estimated percent thrust loss versus deflection angle of bypass stream.

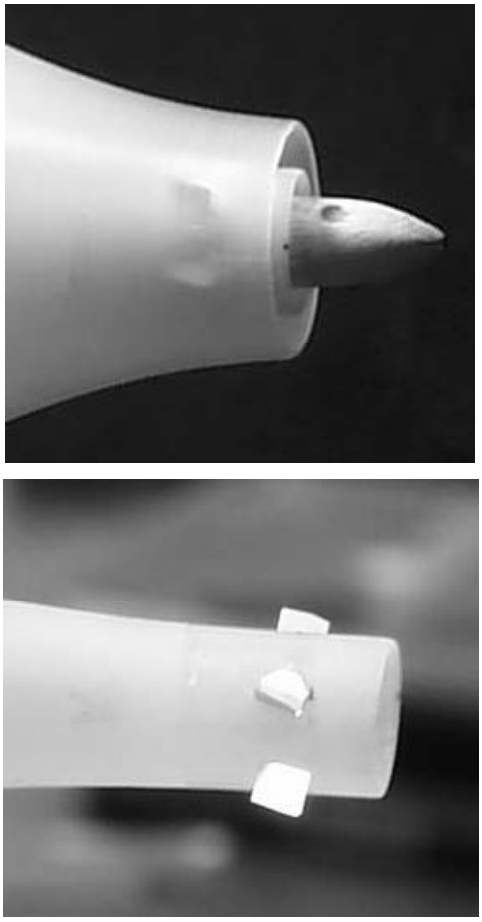

Fig.6 Pictures of the nozzle used in the aeroacoustic tests. Top: assembled nozzle with vanes visible through the translucent nozzle wall. Bottom: vane attachment to inner nozzle.

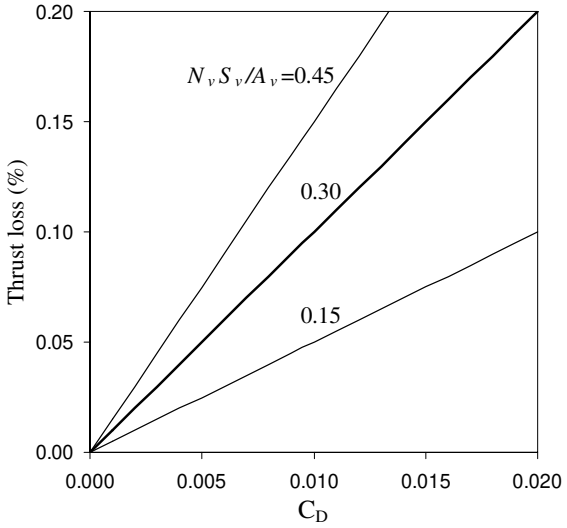

Fig.5 Estimated percent thrust loss at cruise condition with the deflector vanes at zero angle of attack. The heavy line represents the vane configuration of Figs. 6-7.

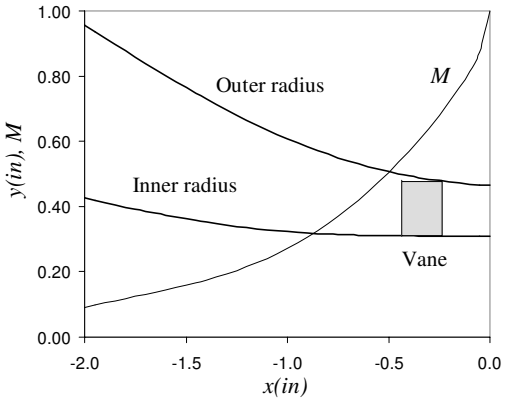

Fig.7 Wall coordinates, placement of vanes, and Mach number distribution in the bypass duct.

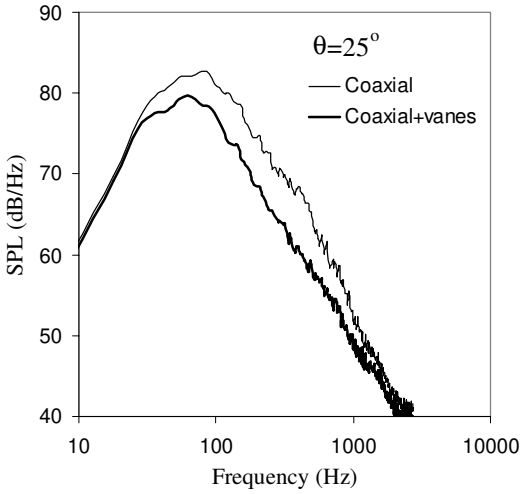

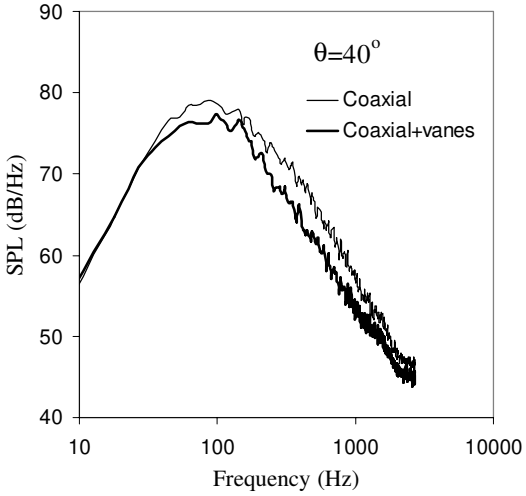

Fig.8 Far-field spectra at polar angles $\theta = 25^\circ$ and 40°. Frequency axis has been scaled to a full-size engine with thrust of 90 kN.

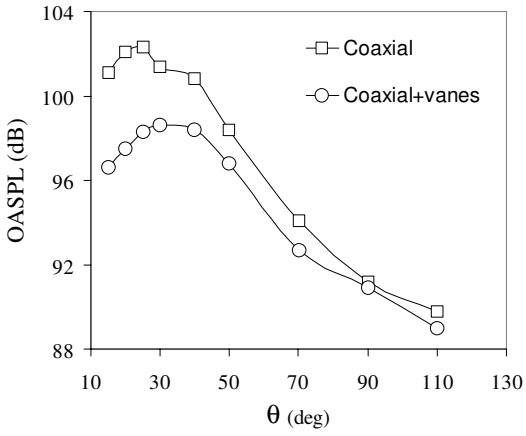

Fig.9 Directivity of overall sound pressure level.

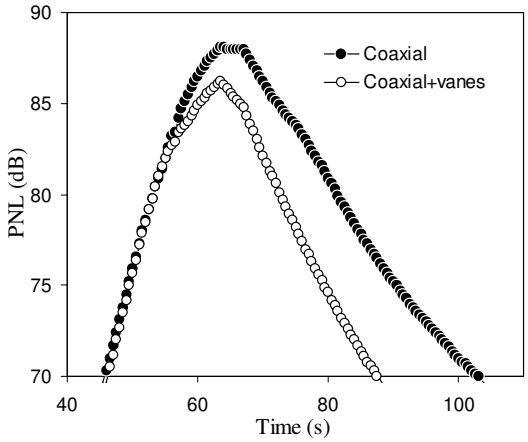

Fig.10 History of perceived noise level recorded by the takeoff monitor.

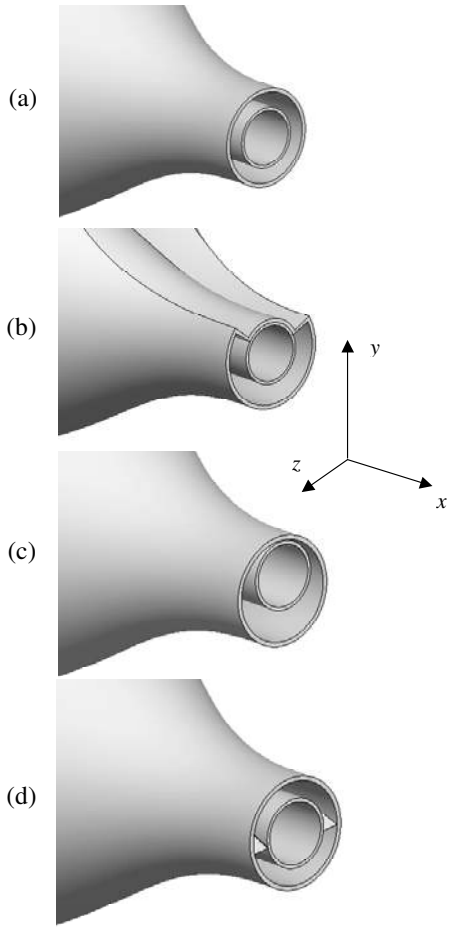

Fig.11 Nozzles used in the mean velocity surveys. (a) coaxial; (b) arcuate; (c) eccentric; (d) coaxial with vanes in the bypass stream. The single jet used the inner nozzle alone. The coordinate system used in the mean flow surveys is shown.

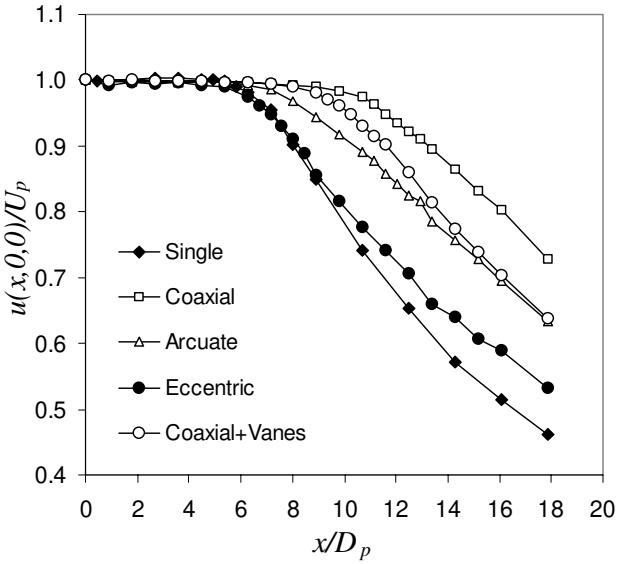

Fig.12 Velocity distribution along the x-axis.

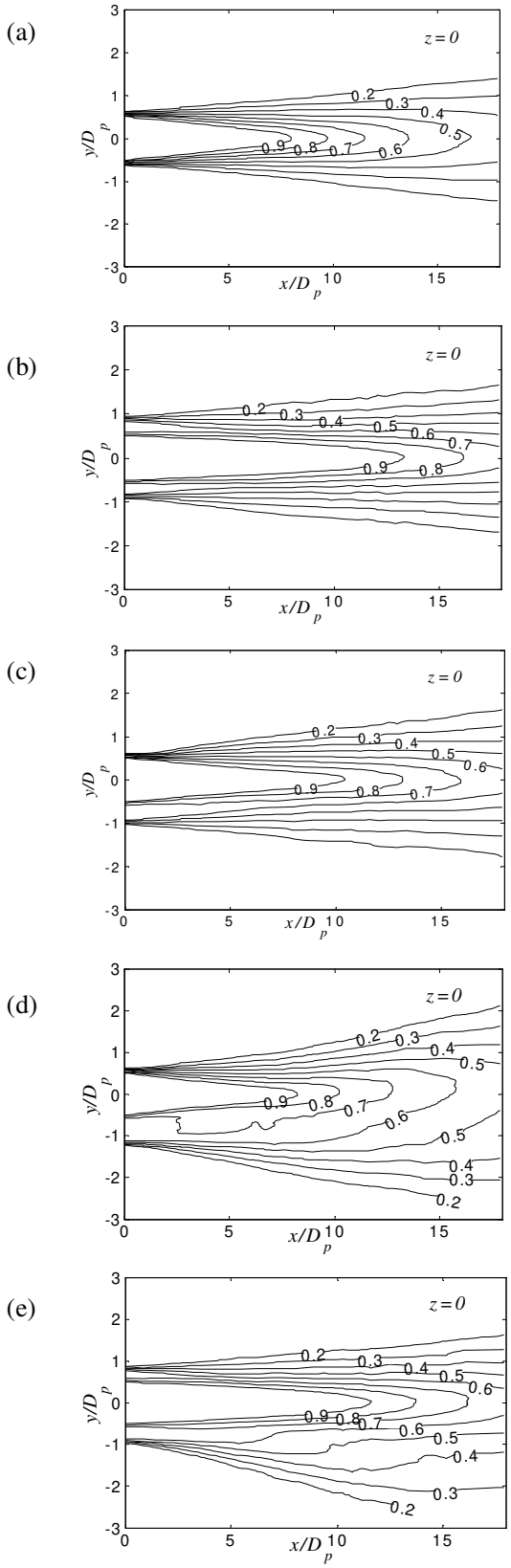

Fig.13 Isocontours of $u(x, y, 0)/U_p$ for all the flows investigated. (a) single; (b) coaxial; (c) arcuate; (d) eccentric; and (e) coaxial with vanes.

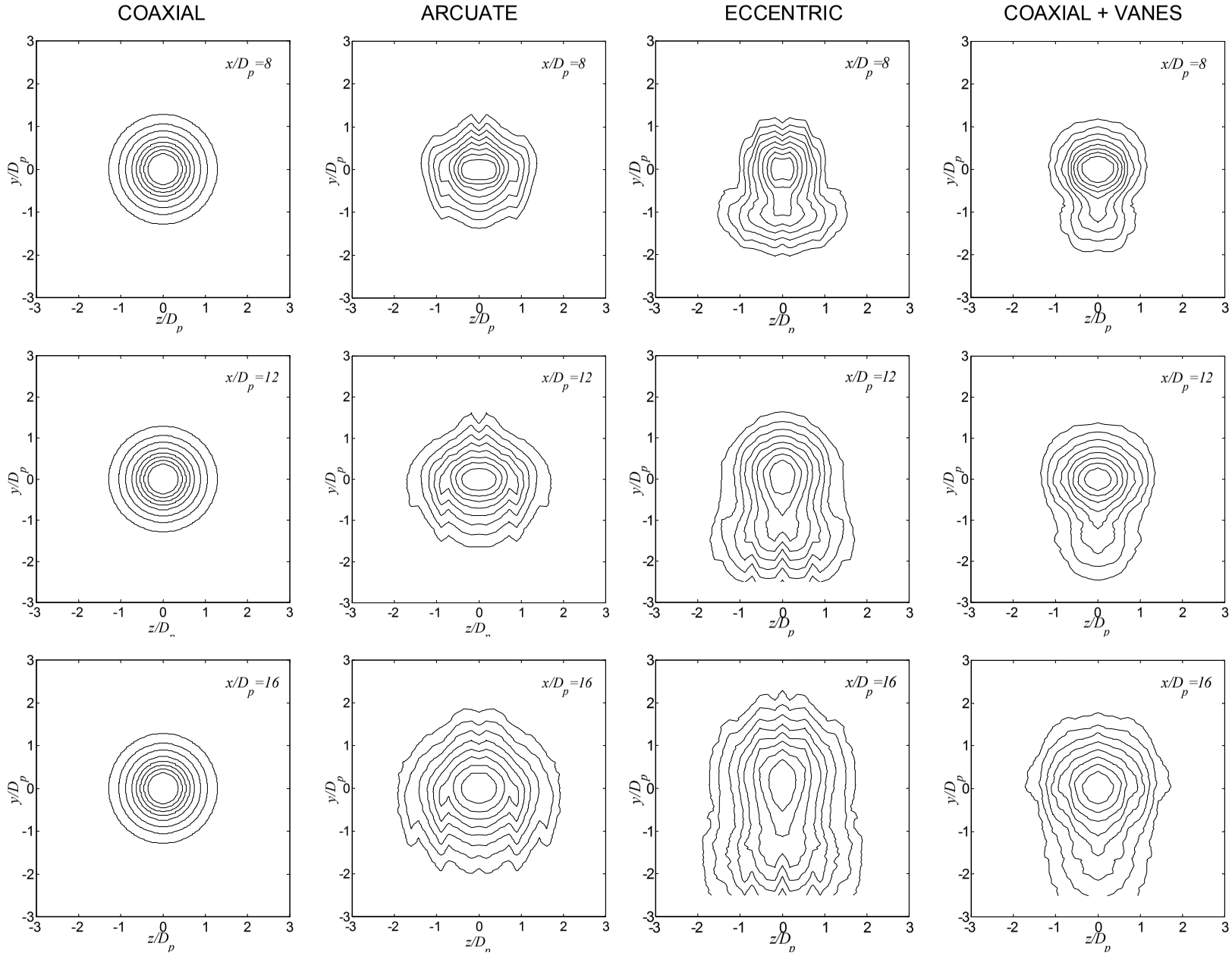

Fig. 14 Isocontours of *u(x,y,z)/u(x,0,0)* at x/D_p=8, 12, and 16. Levels range from 0.2 to 0.9 in increments of 0.1

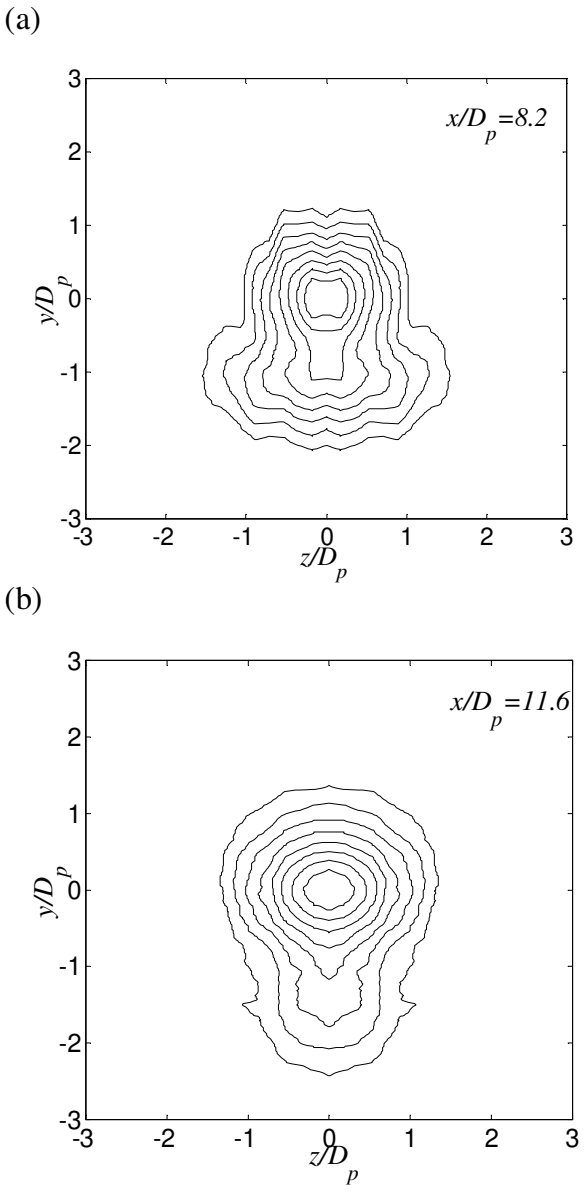

Fig.15 Isocontours of $u(L_p, y, z)/u(L_p, 0, 0)$ of (a) the eccentric jet and (b) the coaxial jet with vanes. Levels range from 0.2 to 0.9 in increments of 0.1.

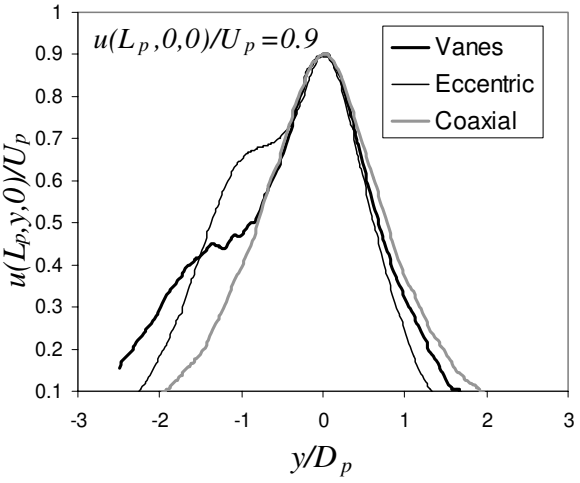

Fig.16 Transverse velocity profiles at the ends of the potential cores of the coaxial, eccentric, and coaxial with vanes jets.